Received: 3 November 2021 | Revised: 10 December 2021 | Accepted: 10 December 2021

DOI: 10.1002/pol.20210813

RESEARCH ARTICLE

JOURNAL OF POLYMER SCIENCE WILEY

Nucleation and crystallization kinetics of polyamide 12 investigated by fast scanning calorimetry

Rui Zhang[1] | **Katalee Jariyavidyanont**[1] | **Mengxue Du**[1] | **Evgeny Zhuravlev**[2] | **Christoph Schick**[2,3] | **René Androsch**[1]

[1]Interdisciplinary Center for Transfer-oriented Research in Natural Sciences (IWE TFN), Martin Luther University Halle-Wittenberg, Halle/Saale, Germany

[2]Institute of Physics and Competence Centre CALOR, University of Rostock, Rostock, Germany

[3]Butlerov Institute of Chemistry, Kazan Federal University, Kazan, Russia

Correspondence
Rui Zhang, Interdisciplinary Center for Transfer-oriented Research in Natural Sciences (IWE TFN), Martin Luther University Halle-Wittenberg, 06099 Halle/Saale, Germany.
Email: rui.zhang@chemie.uni-halle.de

Funding information
Deutsche Forschungsgemeinschaft, Grant/Award Numbers: DFG SPP2122, ZE 661/3-1; Ministry of Education and Science of the Russian Federation, Grant/Award Number: 14.Y26.31.0019

Abstract

Nucleation and crystallization of polyamide 12 (PA 12) have been systematically investigated by fast scanning calorimetry at non-isothermal and isothermal conditions. The critical cooling rates of crystallization and crystal nucleation were determined as 300 and 10,000 K/s, respectively. Moreover, the half-times of nucleation ($t_{1/2,nucl}$) and overall crystallization ($t_{1/2,cry}$) show monomodal and bimodal dependencies on the crystallization temperature. $t_{1/2,nucl}$ has an approximate minimum value of about 0.0005 s at 333 K, which is about 10–20 K above the glass transition temperature, and $t_{1/2,cry}$ has two minima of about 0.05 and 0.8 s at about 333 and 383 K, respectively. Comparing the crystallization behavior of PA 12 with other polyamides, the activation energy for crystallization increases and the energy barrier of short-range diffusion decreases with the increase of the amide-group density in the chains.

KEYWORDS

crystal nucleation, crystallization, fast scanning calorimetry, polyamide 12

1 | INTRODUCTION

Polyamide 12 (PA 12) is a semicrystalline thermoplastic polymer made from ω-aminolauric or laurolactam monomers. It has a long aliphatic chain with 11 methylene groups in the repeat unit separated by an amide group. The long carbon-chain results in a rather low-melting point ($T_{m,0} \approx 500$ K),[1,2] density, and moisture absorption; however, good chemical resistance and dimensional stability, high-elongation at break, and excellent impact resistance compared to other polyamides.[1,3] These properties of PA 12 are similar to polyamide 11 (PA 11), but the cost-performance ratio of PA 12 is better than for PA 11.[4] Therefore, PA 12 is widely used for electronic and engineering applications, as well as for precision hoses and tubes in automotive and some sports goods. PA 12, having these balanced properties, is a superior material for creating functional parts and prototypes utilizing fused deposition modeling (FDM) 3D printing.[5] PA 12 is a semicrystalline polymer, and the final properties of the products will largely depend on the crystallization or processing conditions. Studies of the crystallization kinetics of PA 12 are generally done by differential scanning calorimetry (DSC).[6,7]

However, the limitation to low cooling rates does not allow DSC to access the crystallization of PA 12 at high supercooling of the melt.

Fast scanning calorimetry (FSC) is based on chip-sensor technology, using small samples with masses from sub-nanogram to a few hundreds of nanograms, which largely reduces the total heat capacity of the sample-sensor arrangement. The sample, without a container, is directly placed on the heater. These two factors enable high-scanning rates up to 1,000,000 K/s.[8] By using FSC, the crystallization of polyamides has been intensely investigated.[9–19] As high-cooling rates can be applied, the polyamide melt can be quenched to both low and high supercooling.[9–11,14–18,20–25] The crystallization kinetics can be studied through non-isothermal or isothermal experiments. In addition, the dependencies of the cold-crystallization enthalpy (ΔH_{cc}) on previous cooling rate or time and temperature of crystallization provide an estimate of the nucleation kinetics in non-isothermal and isothermal conditions, respectively.[26]

Several studies applied FSC to investigate the crystallization kinetics of different polyamides.[11,15,16,18,19,24,27–29] A bimodal temperature-dependence of the crystallization rate was observed in most studied polyamides. Li et al. pointed out that hydrogen bonds between the amide groups accelerate crystallization at high temperatures but delay crystallization at low temperatures.[16] Investigation of isothermal crystallization kinetics of PA 12 also yields such bimodal distributions of the half time of crystallization as a function of the crystallization temperature.[13,14] Fischer et al.[20] studied the crystallization behavior of PA 12 according to a temperature–time protocol mimicking processing. They reported that γ and γ′ polymorphs formed at about 333 K and 408 K, respectively. γ is a hexagonal/monoclinic phase and γ′ is a defective γ form (hexagonal phase).[30]

The bimodal dependence of the crystallization rate on temperature has been explained by homogeneous nucleation at high supercooling and heterogeneous nucleation at low supercooling of the melt.[31–35] Rhoades et al.[21] used FSC and X-ray diffraction to investigate the effect of melt-supercooling of PA 11 on heterogeneous and homogenous crystal nucleation. By combining FSC with atomic force microscopy, Zhang et al.[17] measured the rate of homogeneous nucleation of PA 66, which had a maximum value of about 10^{20} m^{-3} s^{-1} at 345 K.

The crystallization kinetics and the positions of the maxima of the overall crystallization rate are different for the large variety of polyamides. The occurrence of one or two minima may be caused by different heterogeneous nuclei densities (impurities) for the different materials. Considering the molecular structure of these polyamides, they exhibit different amide-group densities. In this article, besides a systematic investigation of the kinetics of non-isothermal and isothermal crystal nucleation and crystallization of PA 12 by FSC, the target is to understand the effect of the amide-group density of aliphatic polyamides on these processes.

2 | EXPERIMENTAL STRATEGY

The enthalpy of formation or melting of crystal nuclei is below the detection limit of any calorimetry. Therefore, the direct observation of crystal nuclei by calorimetry is currently impossible. To investigate the crystal nucleation kinetics, Tammann's two-stage crystal nuclei development method is applied, which proposes two separate stages for crystal nucleation and growth.[17,36–38] The nucleation stage allows the formation of crystal nuclei at non-isothermal or isothermal conditions. The subsequent growth stage, which can also be performed at non-isothermal or isothermal conditions, allows the growth of the nuclei formed in the nucleation stage to detectable crystals, allowing indirect observation of crystal nuclei. This way, the nucleation kinetics in the first stage can be analyzed by the non-isothermal or isothermal cold-crystallization enthalpy in the second stage, conveniently assessed by the melting enthalpy of the crystals grown from the nuclei. Figure 1, below, shows the temperature profile for non-isothermal nucleation and non-isothermal crystal growth and consecutive melting. The observed cold crystallization on heating represents the growth stage in Tammann's two-stage method. Figure 5 below shows the profile for isothermal nucleation followed by a

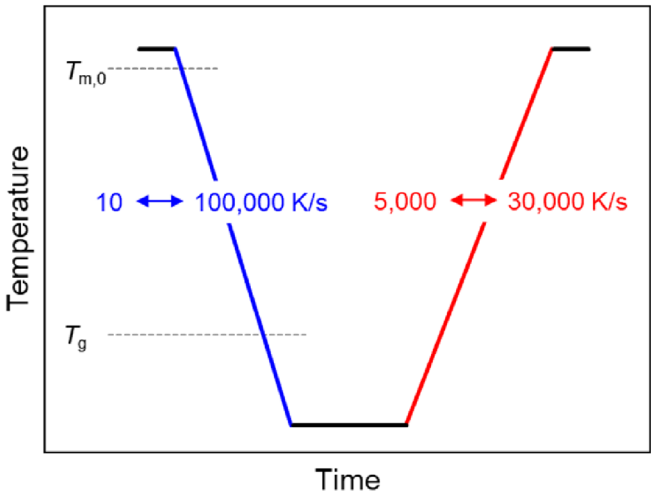

FIGURE 1 Temperature–time protocol for investigating non-isothermal crystallization and nucleation of PA 12 ($T_{m,0}$ = 500 K, T_g = 314 K).[2] PA 12, polyamide 12

non-isothermal growth stage. Again, cold-crystallization on heating represents the growth stage.

3 | MATERIALS AND METHODS

The PA 12 used in this work is a transparent 3D printing grade from Fiberlogy (Poland). It has a melt flow index of 180 cm^3/10 min (508 K/5 kg).

The FSC device (Functional Materials Rostock e.V., Germany) was described elsewhere.[39] A chip-sensor (XI-395, Xensor-Integration, Netherlands)[40] was employed in this work to cover the cooling rate range between 10 and 100,000 K/s and an optimum heating rate range between 5000 and 30,000 K/s for measuring cold crystallization and melting. The sample was cut to obtain a tiny particle and placed on the FSC sensor. A good and stable thermal contact between the sample and the sensor was obtained after several melting-crystallization cycles.[41] Liquid nitrogen was applied as a cooling agent for the thermostat, and gaseous nitrogen provided the thermal link between the chip sensor and the thermostat, as described elsewhere.[39] Before measurement, the thermal history was assured to be erased by heating the material to 540 K, followed by annealing for 0.01 s, which was proven by a preliminary experiment, as shown in supporting materials.

Isothermal crystallization of PA 12 at high temperatures, between 433 and 436 K, was investigated using a Mettler-Toledo heat-flux DSC 1, equipped with the FRS 5 sensor and connected to a Huber intracooler TC100. The purge gas is nitrogen with a flow rate of 60.0 ml/min. The sample, directly being cut from the circular filament into a round section, was placed into an aluminum pan with a volume of 40 µl, and the sample mass was about 4 mg. The temperature and heat flow calibrations of DSC were done by the onset melting temperature and melting enthalpy of indium, respectively.

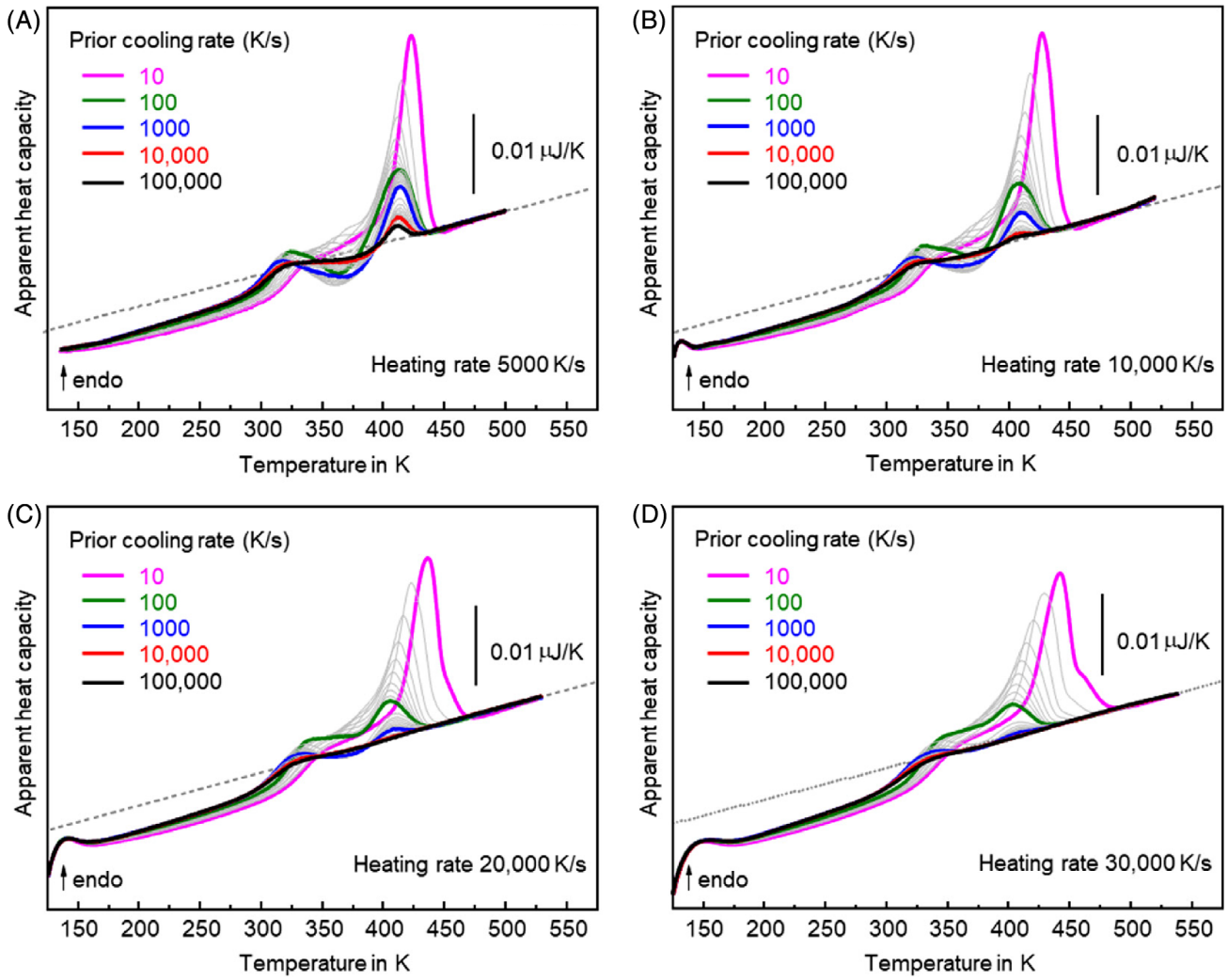

FIGURE 2 FSC heating scans of PA 12 after cooling at different rates between 10 and 100,000 K/s. the heating rates in plots (A), (B), (C), and (D) were 5000, 10,000, 20,000, and 30,000 K/s, respectively. The dashed line represents the heat capacity of the liquid phase, serving as a baseline for obtaining cold-crystallization enthalpies and total enthalpy changes. FSC, fast scanning calorimetry; PA 12, polyamide 12

4 | RESULTS

4.1 | Non-isothermal crystal nucleation and crystallization

Figure 1 shows the thermal protocol of non-isothermal experiments for analysis of the kinetics of crystal nucleation and crystallization of PA 12. The thermal history of the sample was removed at 540 K ($T_{m,0} = 500$ K),[2] where the sample was kept for 0.01 s, which is long enough to equilibrate the nanogram sample.[42,43] Next, the sample was cooled from 540 K to 120 K ($T_g = 314$ K)[2] at different rates varying from 10 to 100,000 K/s (see the blue segment in Figure 1). After equilibrating at 120 K for 0.02 s, the sample was reheated to 540 K at 5000, 10,000, 20,000, or 30,000 K/s (see the red segment in Figure 1). Nuclei and crystal formation during prior cooling at different rates were analyzed from the enthalpies of cold-crystallization and melting in the subsequently recorded heating scans.

Figure 2 shows the FSC heating curves obtained during heating PA 12 at rates of (A) 5000, (B) 10,000, (C) 20,000, and (D) 30,000 K/s after cooling the PA 12 melt at various rates. As the heating rates increase, the available time for crystal growth will become shorter, and then the area of the cold-crystallization peak becomes small. Regarding heating at 5000 K/s (A), quenching the melt with a cooling rate of 100,000 K/s (black curve) shows a glass transition step, a cold-crystallization peak and a melting peak related to melting of crystals formed during cold-crystallization. At cooling rates lower than 10,000 K/s (red curve), the area of the cold-crystallization peak increases due to the increasing number of nuclei formed at slower cooling. When cooling the melt at rates below a few hundred K/s, the cold-crystallization peak area reduces and the melting peak area increases due to the formation of crystals during cooling. If the cooling rates are below 100 K/s, cold-crystallization disappears and the endothermic peak on further heating represents melting of the crystals formed during cooling. With increasing heating rate, the cold-crystallization peaks become smaller, suggesting that the growth of nuclei to crystals was restricted. In addition, the melting peaks become lower in height and broader, which refers to suppression of recrystallization and instrumental thermal lag.[44,45] The thermal-lag related peak-widening will not change the obtained enthalpy values nor the results of the nucleation and crystallization experiments and will therefore not be further discussed.

In Figure 2, the cold-crystallization enthalpy, ΔH_{cc}, was obtained by integrating the area of the cold-crystallization peak. The total change of enthalpy, ΔH_{total}, was obtained by integrating the curves between a temperature slightly above the glass transition to a temperature above the melting peak. In both cases, a linear baseline was used, constructed by extrapolation of the liquid heat capacity to low temperature (see the gray dashed lines in Figure 2).

Figure 3A shows ΔH_{total} as a function of the prior cooling rate, obtained during heating at different rates between 5000 and 30,000 K/s. ΔH_{total} can be used to estimate the crystallization enthalpy during cooling since it is proportional to the fraction of the crystalline phase in the sample. As the cooling rate increases, the value of ΔH_{total} decreases and becomes zero if the cooling rate is higher than 300 K/s, indicating the critical value for suppression of crystallization. As expected, the variation of the heating rate used in the measurement scan (red segment in Figure 1) has no noticeable effect on the dependence of ΔH_{total} on cooling rate. It is worth noting, although ΔH_{total} as a function of cooling rate is not affected by the heating rate, the structure of the melting peak is still significantly influenced by the heating rate because of recrystallization.[46–49]

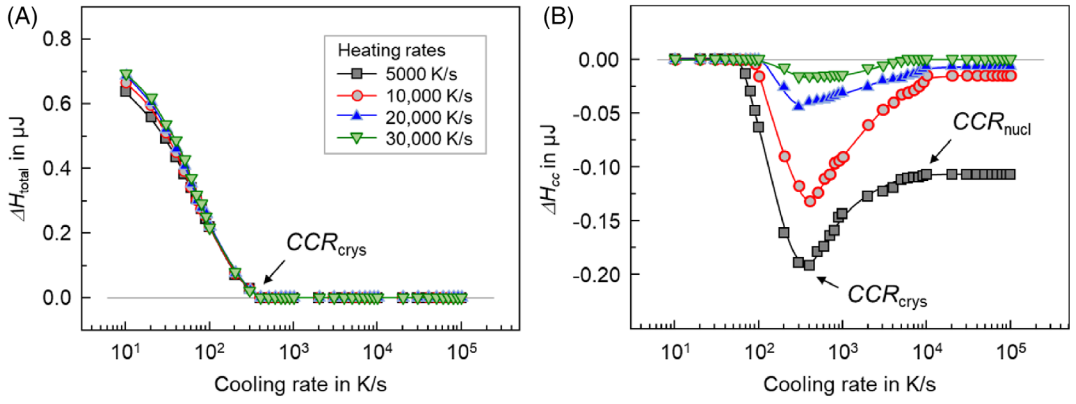

FIGURE 3 (A) ΔH_{total} and (B) ΔH_{cc} as a function of prior cooling rate between 10 and 100,000 K/s

Figure 3B shows ΔH_{cc} as a function of prior cooling rate, obtained during heating the samples at different rates. The values of ΔH_{cc}, evaluated from the area of the cold-crystallization peaks, are used to estimate the non-isothermal nucleation kinetics. It increases when the cooling rate is above 80 K/s. The increase of ΔH_{cc} here refers to the suppression of crystallization during cooling. Cooling the melt at a rate higher than 300–400 K/s decreases ΔH_{cc} due to the suppression of homogeneous nucleation, which leads to a decrease of the number of available nuclei.[17,18,26,50] Increasing the cooling rate to above 10,000 K/s, the value of ΔH_{cc} becomes zero or constant at a certain value. The latter is detected if using heating rates lower than 10,000 K/s, presumably due to the presence of heterogeneous nuclei. Homogeneous nucleation is entirely suppressed if cooling the sample at rates faster than 10,000 K/s. For heating rates of 5000 and 10,000 K/s, the value of ΔH_{cc} finally cannot reach a value near zero, which will be further analyzed in the next section.[18,26]

As described in the introduction, the cold-crystallization enthalpy is proportional to the nuclei number as well as the time available for growth during reheating; as such, the cold-crystallization enthalpy is highly dependent on the cooling and heating rates applied. When the heating rate is low, the value of ΔH_{cc} becomes constant on cooling at rates above 10,000 K/s because a small number of unavoidable heterogeneous nuclei initiates cold crystallization. Two critical cooling rates, corresponding to the suppression of growth of nuclei (i.e., of crystallization) and homogenous crystal nucleation, respectively, are illustrated in Figure 3A,B for PA 12, marked as black arrows in the corresponding figure. The first critical cooling rate (CCR_{crys}) is the cooling rate where ΔH_{total} reaches zero, and the second critical cooling rate (CCR_{nucl}) is the cooling rate where the cold-crystallization enthalpy reaches zero or becomes constant. CCR_{crys} and CCR_{nucl} are determined as about 300 and 10,000 K/s, respectively. Li et al. reported that ΔH_{total} of PA 12 decreases to zero on cooling faster than 500 K/s,[16] which agrees with our result.

4.2 | Critical heating rate of PA 12

If the heating rate is suitable, the formation and growth of nuclei can occur during heating.[26,50] The crystallization behavior of PA 12 at different heating rates is investigated through the temperature–time protocol shown in Figure 1 with a fixed cooling rate of 100,000 K/s. At first, the sample is quenched from 540 K to 120 K by cooling at 100,000 K/s. According to the results shown above, crystallization and homogeneous crystal nucleation are absent at this cooling rate. After equilibrating at 120 K for 0.02 s, the sample is reheated to 540 K at different heating rates varying from 1000 to 30,000 K/s (red segment), which is used to analyze the crystallization behaviors during heating via the cold-crystallization enthalpy.[50] Because the sample is quenched, any nuclei in the sample are heterogeneous nuclei or homogeneous nuclei formed during heating. As such, the value of ΔH_{cc} will be influenced by both homogeneous and heterogeneous nucleation.

Figure 4A shows the heating scans (see the red segment in Figure 1) of PA 12 with heating rates varying from 1000 to 30,000 K/s. Regarding the heating scan at 1000 K/s, a cold-crystallization peak and a subsequent melting peak were observed with the same area, indicating a crystal-free structure in the sample before heating. As the temperature increases during heating, the nuclei first grow to crystals and then these crystals melt, causing cold-crystallization and melting peaks, respectively. As

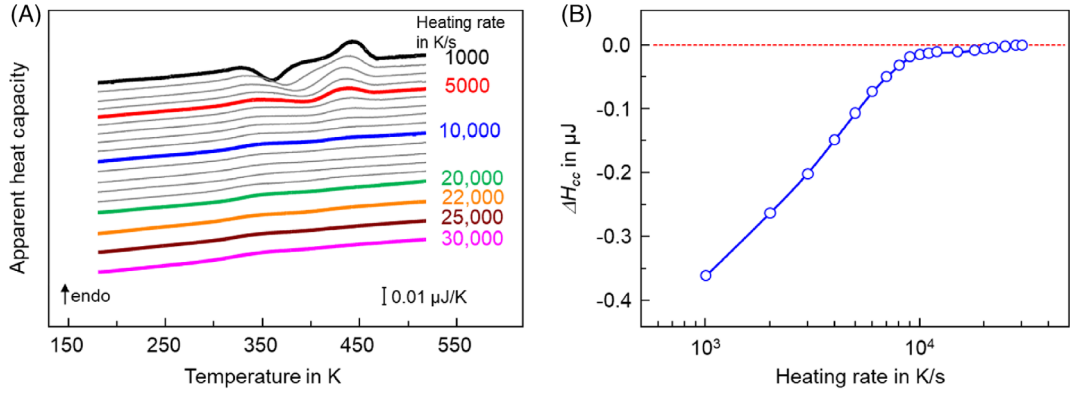

FIGURE 4 (A) FSC heating scans of PA 12, which was quenched to 120 K at 100,000 K/s, recorded at different heating rates varying from 1000 to 30,000 K/s. (B) Cold-crystallization enthalpy (ΔH_{cc}), of scans shown in (A), as a function of heating rate. FSC, fast scanning calorimetry; PA 12, polyamide 12

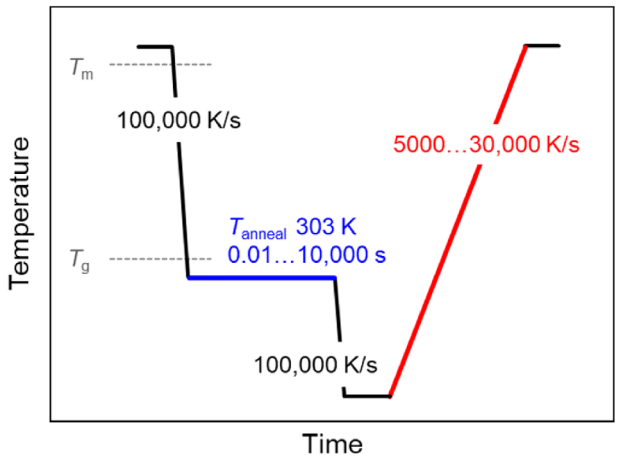

FIGURE 5 Thermal protocol for investigating the isothermal nucleation and crystallization kinetics of PA 12 ($T_{m,0} = 500$ K, $T_g = 314$ K).[2] PA 12, polyamide 12

the heating rate increases, the areas of the cold-crystallization and melting peaks become smaller. The cold-crystallization enthalpy as a function of the heating rate is shown in Figure 4B. It decreases with heating rate and reaches a value close to zero at 10,000 K/s. The critical heating rate (*CHR*) is the heating rate above which cold-crystallization is suppressed during heating. C*HR* is about 10,000 K/s. It is worth noting that there is still a small residual enthalpy at 10,000 K/s in Figure 4B. Above 10,000 K/s, the decrease of cold-crystallization enthalpy becomes significantly slower; therefore, cold-crystallization is assumed to be suppressed at this heating rate. This experiment alone does not allow us to decide if the effect is caused by missing homogeneous nucleation on heating or a too short time for a detectable growth of crystals from nuclei formed on heating. A distinction between both explanations becomes possible with a sample containing nuclei before heating at the *CHR*. In Figure 3B, the red curve corresponds to heating at the *CHR* of 10,000 K/s, and for prior cooling rates below 100,000 K/s homogeneous nuclei are formed during cooling, see above. The observed cold-crystallization enthalpy in Figure 3B shows that crystal growth from pre-existing nuclei is possible at the *CHR* and even at higher heating rates of 20,000 and 30,000 K/s. Consequently, missing nucleation on heating causes the disappearance of the cold-crystallization peak for a sample cooled faster than the CCR_{nucl} (negligible number of nuclei) on heating at or above the *CHR*

The peak maximum of the cold crystallization peak asymptotically approaches about 400 K. According to the derivations provided in ref. 51, this temperature is close to the maximum of the crystal growth rate.

4.3 | Isothermal crystal nucleation and crystallization

The kinetics of homogeneous crystal nucleation at high supercooling of the melt is analyzed using isothermal nucleation and Tammann's two-stage crystal nuclei development method employing a non-isothermal growth stage. Figure 5 shows the temperature–time protocol for investigating the isothermal nucleation and crystallization kinetics at 303 K. At this temperature, around 10 K below T_g, homogeneous nucleation and crystal growth are slow and well separated in time, allowing to follow both separately by FSC. The sample is cooled from 540 K to 303 K at the maximum possible cooling rate of the chip-sensor (100,000 K/s) and then isothermally annealed at 303 K for different times. After the isothermal segment, the sample is cooled to 120 K at 100,000 K/s. Finally, the sample is reheated to 540 K at 5000, 10,000, 20,000, and 30,000 K/s (red segment), which is applied to evaluate isothermal nucleation and crystallization.

Figure 6 shows the heating curves corresponding to the red segment in Figure 5. Regarding the data obtained on heating at 5000 K/s (Figure 7A), the heating scan of the sample annealed for 0.01 s (the black curve) shows, from low to high temperatures, the glass transition step, a cold-crystallization peak, and a melting peak related to crystals formed during cold-crystallization. As the annealing time increases, the cold-crystallization and melting peaks increase in size due to an increase of the nuclei number. However, increasing the annealing time above 1 s (red curve), two overlapping events, enthalpy recovery and melting of tiny crystals formed during annealing, occur at low temperatures. Therefore, the endothermic peak at the glass transition is larger than the endothermic peak observed after shorter annealing. Noteworthy, the exothermic peak does no longer represent cold-crystallization only but also crystal reorganization on further heating. As the heating rate increases, the melting peaks at high temperatures become smaller due to reduced cold crystallization and broader due to smearing at the highest heating rate (30,000 K/s), similar to Figure 2. The relatively sharp low-temperature melting peak also broadens due to smearing with increasing heating rate already at 10,000 K/s. However, both effects, reduced cold crystallization and smearing, do not influence the total enthalpy change of PA 12, as shown in Figure **7**A.

The values of ΔH_{total} and ΔH_{cc} as a function of annealing time are shown in Figure 7A,B, respectively. In Figure 7A, ΔH_{total} increases if annealing the sample longer than about 0.2 s, indicating the onset of crystal growth during the isotherm. Different heating rates do not influence the values of ΔH_{total} and its dependence on

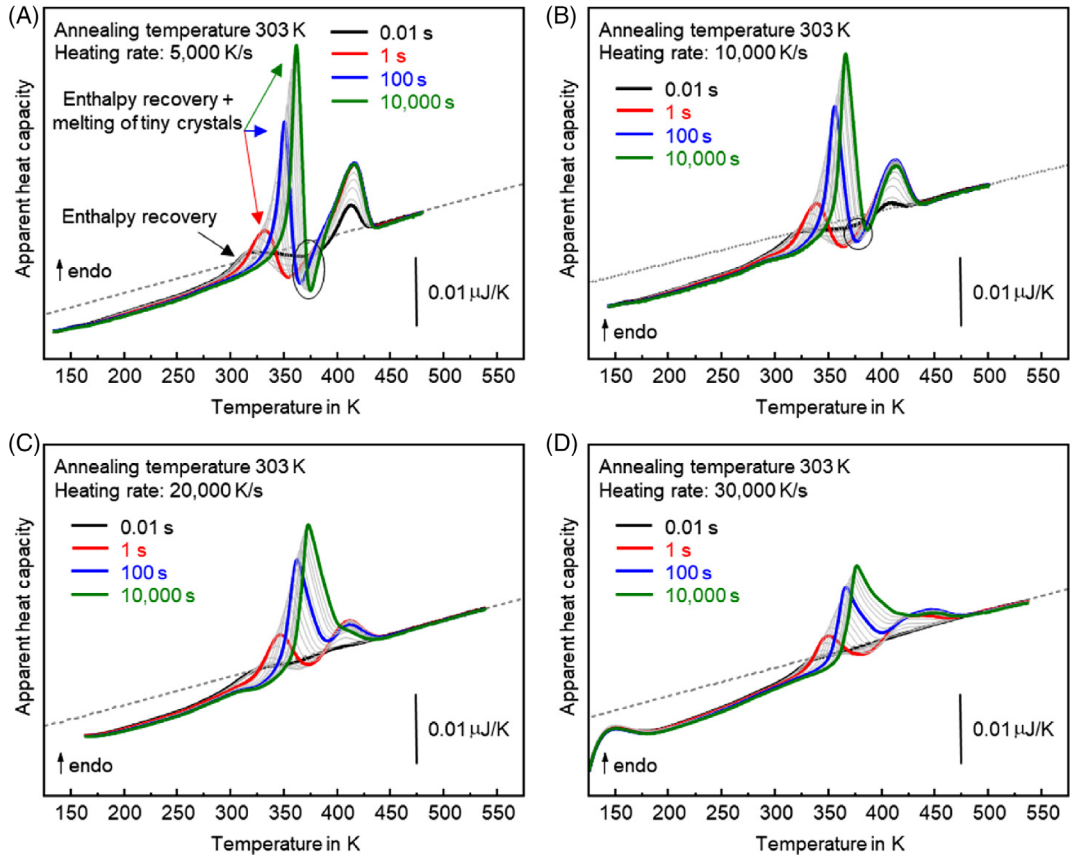

FIGURE 6 FSC heating scans of PA 12 after isothermal annealing at 303 K with the annealing time varying from 0.01 to 10,000 s. the heating rates in plots (A), (B), (C) and (D) were 5000, 10,000, 20,000, and 30,000 K/s, respectively. FSC, fast scanning calorimetry; PA 12, polyamide 12

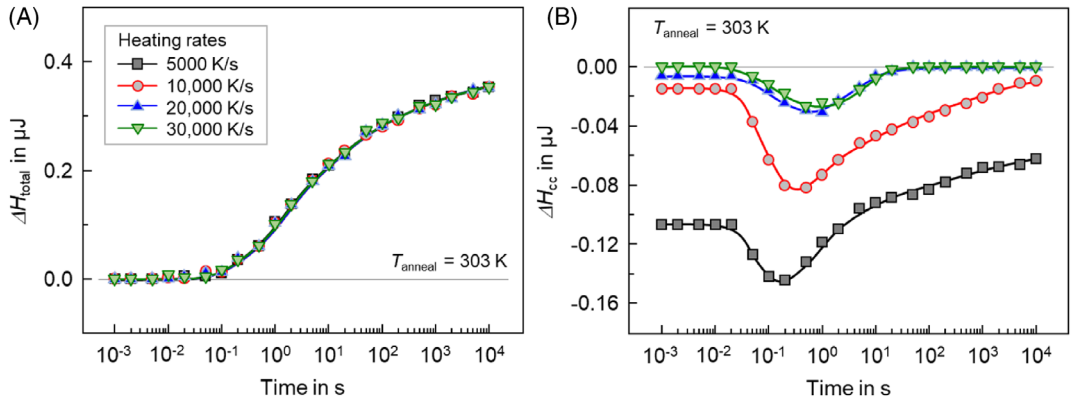

FIGURE 7 (A) ΔH_{total} and (B) ΔH_{cc} as a function of annealing time at 303 K for different heating rates

annealing time. In Figure 7B, the value of ΔH_{cc} increases at first if the sample is annealed longer than about 0.02 s and then decreases if the annealing time is longer than about 0.5 s. The increasing number of homogeneously formed nuclei causes the increasing values and the decreasing values are due to the decreasing volume available for crystal growth on heating because of the space occupied by the crystals already grown during the isotherm.[17,18,26,52,53] Unlike ΔH_{total}, the values of ΔH_{cc} are highly dependent on the heating rate; even the annealing time dependency is qualitatively similar.[17,37,38,54] After reaching the maximum, the trends for heating rates of 5000 and 10,000 K/s are different from the trends of heating rates of 20,000 and 30,000 K/s because crystallization during the isotherm causes increasing recrystallization, which cannot be distinguished from cold crystallization at the low-heating rates.[34,46,47] Recrystallization is suppressed at high-heating rates, and the

exothermic peak finally disappears. Based on the above discussion, the heating rate of 30,000 K/s will be applied to studying isothermal nucleation and crystallization kinetics for different temperatures. From Figure 7B, it follows that at 303 K, nucleation can only be followed between 0.01 and 1 s because of superimposed crystallization at longer times.

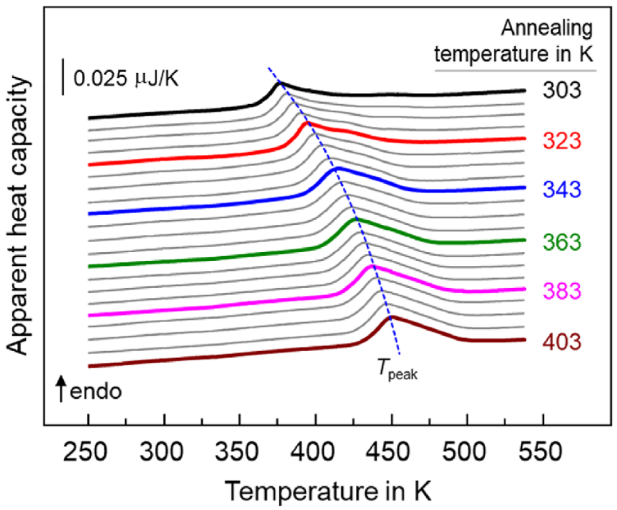

FIGURE 8 FSC heating curves after isothermal annealing between 303 and 403 K for 10,000 s. the heating rate for all curves is 30,000 K/s. The blue dash line is a guide for the eye. FSC, fast scanning calorimetry

The kinetics of isothermal nucleation and crystallization in the temperature range from 303 to 403 K (with an increment of 5 K) is investigated through the thermal protocol shown in Figure 5. The sample was cooled from 540 K to different isothermal crystallization temperatures at 100,000 K/s and crystallized at these temperatures for different times. When the isothermal annealing segment was finished (green segment), the sample was cooled to 120 K at 100,000 K/s. After equilibrating at 120 K for 0.02 s, the sample was reheated to 540 K at 30,000 K/s, serving as an analysis scan (red segment in Figure 5).

The heating curves after crystallization at different crystallization temperatures for 10,000 s are shown in Figure 8. The melting peak shifts to higher temperatures as the crystallization temperature increases. According to the results of Figure 7, the asymmetry in the melting peaks is due to recrystallization.

ΔH_{total} and ΔH_{cc} obtained at different T_c as a function of crystallization time are shown in Figure 9A,B. The half-times of nucleation ($t_{1/2,nucl}$) and crystallization

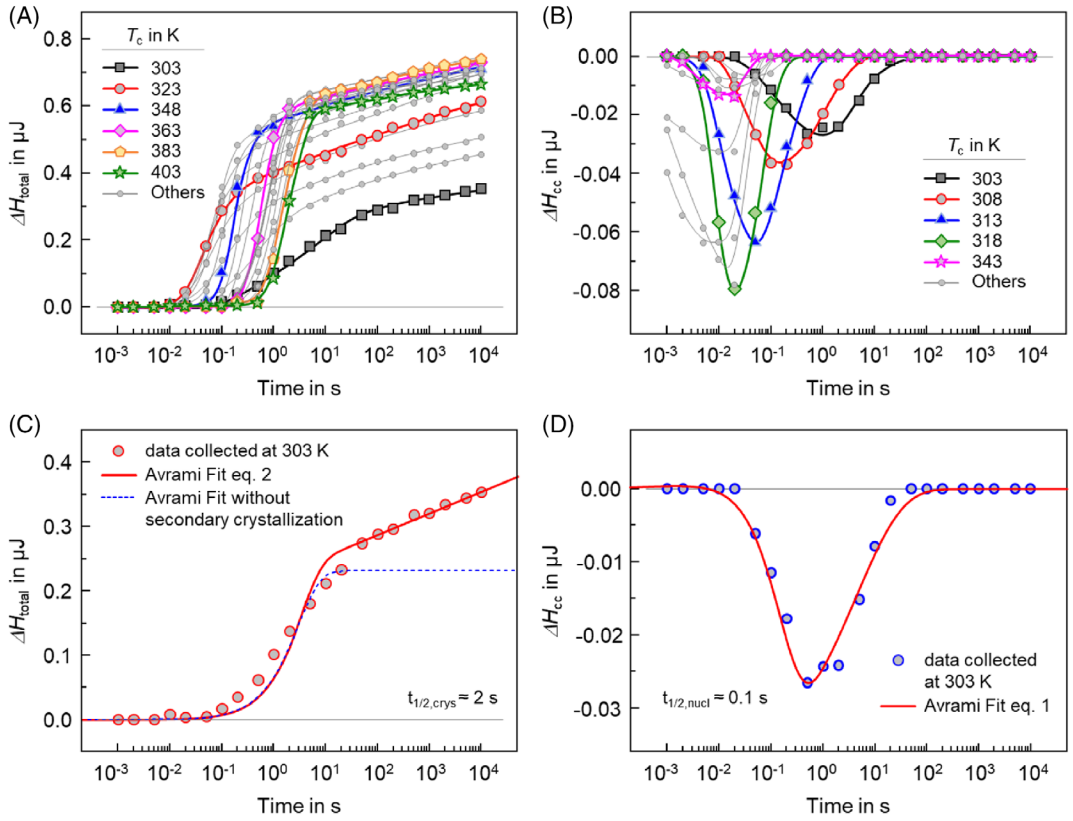

FIGURE 9 (A):ΔH_{total} obtained at different T_c as a function of crystallization time. (B) ΔH_{cc} obtained at different T_c as a function of crystallization time. (C) An example of fitting the data to describe the dependence of ΔH_{total} on crystallization time. (D) An example of fitting the data to describe the dependence of ΔH_{cc} on crystallization time. The heating rate is 30,000 K/s

($t_{1/2,crys}$) are estimated through a fit of the two data sets, with the fitting functions represented by Equations (1) and (2), respectively.[17,26,55–57] The half time of nucleation, $t_{1/2,nucl}$, and overall crystallization, $t_{1/2,crys}$, reflect the inverse of the rate of nucleation and crystallization, respectively, at a particular T_c.

$$\Delta H_{cc} = -\left(\Delta H_{nucl}\left(1-\exp\left(-\frac{t}{t_{\frac{1}{2},nucl}}ln2\right)^n\right)+\Delta H_{het}\right) + \Delta H_{total}. \quad (1)$$

$$\Delta H_{total} = \Delta H_{crys}\left(1-\exp\left(-\frac{t}{t_{1/2,crys}}ln2\right)^n\right) + A_2\left(ln\left(t-t_{1/2,crys}\right)\right) * \left(\frac{1}{2}\frac{\left|t-t_{\frac{1}{2},crys}\right|}{t-t_{\frac{1}{2},crys}}+1\right). \quad (2)$$

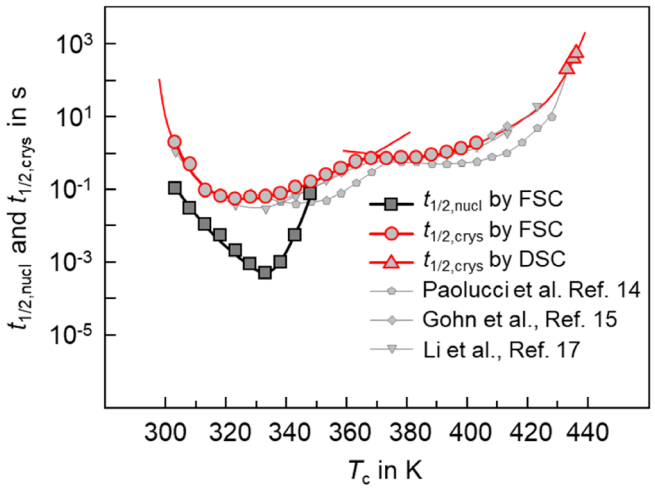

FIGURE 10 $t_{1/2,nucl}$ and $t_{1/2,crys}$ as a function of T_c. Additional half-times of crystallization data are obtained from ref. 13,14,16, shown by gray symbols. Data represent averages of two measurements, with the error bars being smaller than the symbol size

In Equations (1) and (2), ΔH_{nucl} is the maximum cold-crystallization enthalpy due to the formation of homogenous nuclei, ΔH_{crys} is the final enthalpy of the primary crystallization, t is the annealing time, and n and A_2 are constants. ΔH_{het} is the enthalpy change due to cold crystallization at the chosen heating rate on heterogeneities. The data at $T_c = 303$ K are used as an example of determining $t_{1/2,crys}$ and $t_{1/2,nucl}$, which are shown in Figure 9C,D, respectively.

In Figure 10, a bimodal temperature-dependence of $t_{1/2,crys}$ as a function of crystallization temperature is observed, which corresponds to the temperature dominance of homogeneous and heterogeneous nucleation, respectively.[31–35] At low temperatures/high melt-supercooling, homogeneous nuclei form and dominate crystallization. However, at low supercooling, the homogeneous nucleation rate is extremely low. Then the number of homogeneous nuclei is much smaller than the number of heterogeneous nuclei, and heterogeneous nucleation becomes dominant. The two minimum values of $t_{1/2,crys}$ are evident at 333 K, being around 0.05 s, and 383 K, being around 0.8 s. The values of $t_{1/2,crys}$ are similar to literature data,[13,14,16] plotted as gray curves in Figure 10. The small difference in $t_{1/2,crys}$ to Paolucci et al.[13] might be due to (i) crystal growth during slow heating and/or previous slow cooling, (ii) different polymer grades, and (iii) impurities that act as heterogeneous nucleation sites.

In addition, $t_{1/2,nucl}$ is shown in Figure 10 as a function of T_c at temperatures between 303 and 348 K. As T_c decreases, $t_{1/2,nucl}$ decreases at first and then increases, revealing a minimum at 333 K, being around 0.0005 s. The position of the minimum is controlled by the interplay of the increase of the thermodynamic driving force for crystal nucleation with supercooling and the decrease of short-range diffusion ability of molecular segments.[31,58–62]

TABLE 1 Critical cooling rates to suppress crystals nucleation and crystallization in polyamides of different amide-group concentration

Polymer	N_{-CH2-}	CCR_{crys} (K/s)	CCR_{nucl} (K/s)	Reference
PA 6	5	500		63
		150		24
		100		25
PA 66	5.5	750		22
PA 11	10	500	30,000	11
		1000		18
PA 12	11	500		16
		300	10,000	Present work

Abbreviations: CCR, critical cooling rate; PA, polyamide.

5 | DISCUSSION

5.1 | Non-isothermal nucleation and crystallization

In this study, CCR_{crys} and CCR_{nucl} of PA 12 are determined as 300 and 10,000 K/s, respectively. In order to evaluate and discuss the specific crystallization behavior of PA 12, a comparison with different polyamides is advised. Data of CCR_{crys} and CCR_{nucl} of PA 6, PA 66, PA11, and PA 12, available in the literature, are listed in Table 1. The amide-group density is quantified by the average number of —CH_2— groups between two adjunct amide groups (N_{-CH2-}) and correlated with the crystallization behavior. CCR_{crys} and CCR_{nucl} are plotted as a function of N_{-CH2-} in Figure 11. Even though data are lacking, it can be seen that CCR_{crys} of all polyamides

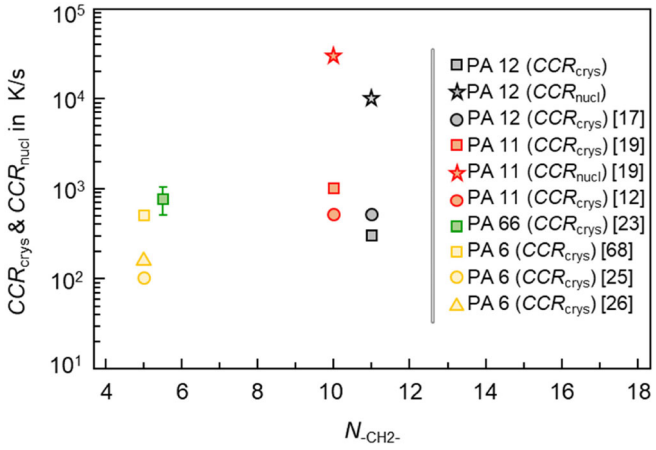

FIGURE 11 First (CCR_{crys}) and second (CCR_{nucl}) critical cooling rate of polyamides as a function of the average number of —CH_2— groups between two adjunct amide groups (N_{-CH2-}). The source of data is described in the legend. CCR, critical cooling rate

TABLE 3 Available glass transition temperatures and equilibrium melting temperatures in the literature

Polymer	T_g (K)	Reference	$T_{m,0}$ (K)	Reference
PA 46	345 K	64	563 K	64
PA 6	313 K	65	533 K	65
PA 66	323 K	66	574 K	66
PA 610	323 K	67	506 K	67
PA 612	319 K	68	520 K	68
PA1012	301 K	16	479 K	16
PA 11	316 K	69	493 K	69
PA 12	314 K	2	500 K	2

Abbreviation: PA, polyamide.

TABLE 2 Available isothermal crystallization parameters of polyamides from literatures

Polyamide	N_{-CH2-}	$T_{crys,low\text{-}T\ minimum}$ (K)	$t_{1/2,crys,low\text{-}T\ minimum}$ (s)	$T_{crys,high\text{-}T\ minimum}$ (K)	$t_{1/2,crys,high\text{-}T\ minimum}$ (s)	$T_{nucl,minimum}$ (K)	$t_{1/2,nucl}$ (s)	Reference
PA 46	4	413	0.01	463	0.06			16
PA 6	5	368	4	413	1			15
		368	3	413	0.8			24
				413	1			28
				413	1			29
PA 66	5.5	385	0.4	445	0.3	335	0.02	19
		393	0.2	445	0.5			17
		393	0.4					16
PA 610	7	353	0.8	403	0.8			16
PA 612	8	353	1.5	403	0.6			16
PA 1012	10	333	0.06	383	0.5			16
PA 11	10	333	0.05	403	3	333	≈0.01	18
		340	0.05	400	2			11
PA 12	11	333	0.05	383	0.8	333	0.0005	Present work
		333	0.04	383	0.7			
		343	0.02	393	0.8			16
				383	0.75			13
								14

Note: $T_{crys,low\text{-}T\ minimum}$ and $T_{crys,high\text{-}T\ minimum}$ are the temperatures corresponding to the minimum $t_{1/2,crys}$ as a function of temperature at high and low temperatures, respectively. $T_{nucl,minimum}$ is the temperature corresponding to the minimum $t_{1/2,nucl}$ as a function of temperature.
Abbreviation: PA, polyamide.

considered are of the same order of magnitude between about 10^2 and 10^3 K/s. No conclusion can be made here from such a limited data set.

5.2 | Isothermal nucleation and crystallization kinetics

Literature data of the minima of $t_{1/2,crys}$ and $t_{1/2,nucl}$ and the corresponding temperatures are listed in Table 2. Because the temperatures of minimum $t_{1/2,crys}$ and $t_{1/2,nucl}$ are controlled by the supercooling and short-range diffusion,[58,59] two reduced temperatures, that is, $(T_{m,0}\text{-}T_{min})/(T_{m,0}\text{-}T_g)$ and $(T_{min}\text{-}T_g)/(T_{m,0}\text{-}T_g)$, are used to uniformly scale the data and to compare these polyamides; T_{min} is the temperature at the minimum of $t_{1/2,crys}$ or $t_{1/2,nucl}$. For calculation of these two reduced temperatures, $T_{m,0}$ and T_g are required and are taken from references, as listed in Table 3.

Figure 12A shows the low-temperature minimum of $t_{1/2,crys}$ of different polyamides as a function of $N_{\text{–CH2–}}$ It decreases as $N_{\text{–CH2–}}$ increases. According to ref. 70, the properties of polyamides become more similar to polyolefins with the decrease of the amide-group density, and then, the crystallization becomes faster; only PA 46 is an exception of the observed trend, for unknown reasons. Due to the possible presence of additives, plasticizers, and so forth, validation of the crystallization behavior of PA 46 still is needed. In addition, at high temperatures, there is no obvious trend for the dependence of $t_{1/2,crys}$ on $N_{\text{–CH2–}}$, which is expected due to predominant heterogeneous nucleation. As such, crystallization at these temperatures is largely determined by the specific grades used for the experiment. This way, the crystallization behavior at high temperatures is not further discussed here. Furthermore, $(T_{m,0}\text{-}T_{min})/(T_{m,0}\text{-}T_g)$ and $(T_{min}\text{-}T_g)/(T_{m,0}\text{-}T_g)$ obtained at the low-temperature minimum is plotted as a function of $N_{\text{–CH2–}}$ in Figure 12B. As $N_{\text{–CH2–}}$

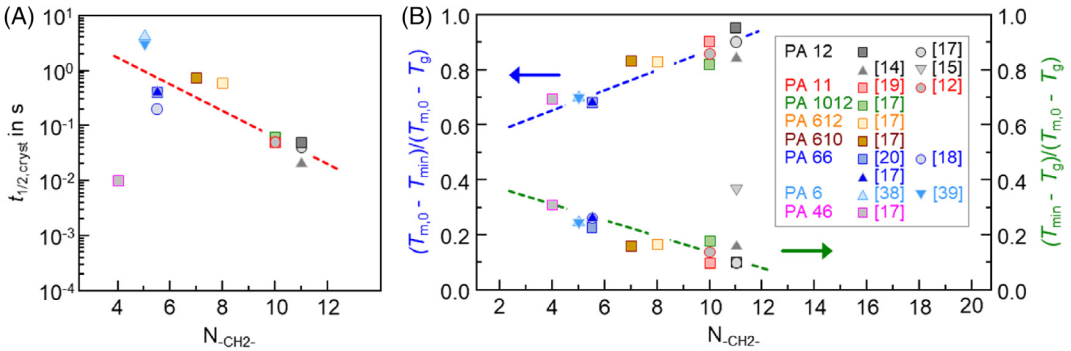

FIGURE 12 (A) Low-temperature minimum of the half-time of crystallization ($t_{1/2,crys}$) as a function of the average number of —CH_2— groups between two adjunct amide groups ($N_{\text{–CH2–}}$). (B): Temperature T_{min} of the low-temperature minimum of $t_{1/2,crys}$ normalized regarding $T_{m,0}$ and T_g as a function of $N_{\text{–CH2–}}$

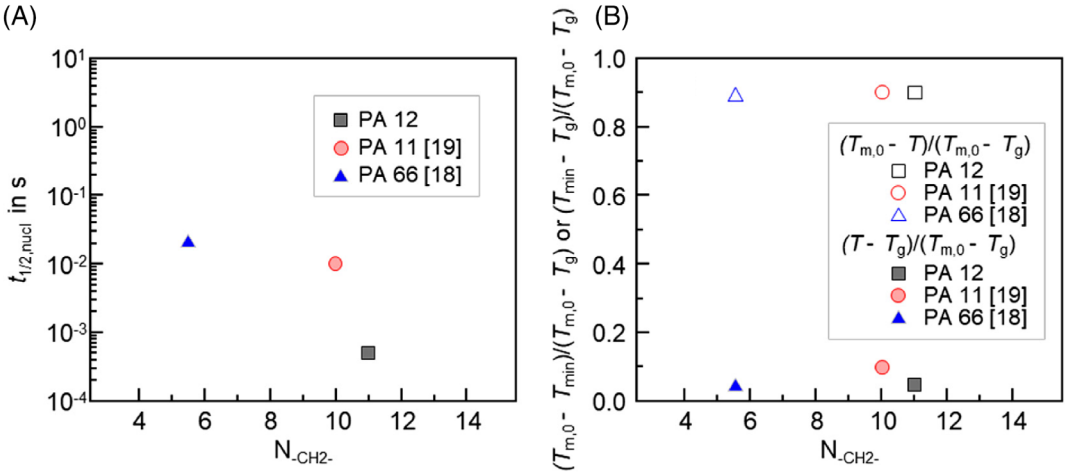

FIGURE 13 (A) Minimum values of the half-time of nucleation, $t_{1/2,nucl}$, as function of the average number of —CH_2— groups between two adjunct amide groups ($N_{\text{–CH2–}}$). (B) Temperature T_{min} of the minimum of $t_{1/2,nucl}$ normalized regarding $T_{m,0}$ and T_g as a function of $N_{\text{–CH2–}}$, indicated with open- and solid symbols, respectively

increases, $(T_{m,0}\text{-}T_{min})/(T_{m,0}\text{-}T_g)$ correspondingly increases, but $(T_{min}\text{-}T_g)/(T_{m,0}\text{-}T_g)$ decreases. This result indicates that the required activation energy of crystallization increases and the energy barrier of short–range diffusion decreases with increasing $N_{\text{–CH2–}}$. It has been reported in the literature that an increasing amide-group density in polyamides decreases the entropy of the melt, thus favoring perhaps homogeneous crystal nucleation.[71–74] In addition, more —CH_2— groups between two adjunct amide groups make molecules more flexible, which is beneficial for diffusion. So, the energy barrier of short-range diffusion reduces. The molecular structure of PA 12 ($N_{\text{–CH2–}} = 11$), therefore, causes a rather low-activation energy of crystallization

Figure 13A shows $t_{1/2,nucl}$ of PA 66, PA 11, and PA 12 as function of $N_{\text{–CH2–}}$, yielding a sequence of PA 12 < PA 11 < PA 66. Figure 13B shows the dependencies of $(T_{m,0}\text{-}T)/(T_{m,0}\text{-}T_g)$ and $(T\text{-}T_g)/(T_{m,0}\text{-}T_g)$ on $N_{\text{–CH2–}}$. Unlike in Figure 12B, the values of $(T_{m,0}\text{-}T)/(T_{m,0}\text{-}T_g)$ and $(T\text{-}T_g)/(T_{m,0}\text{-}T_g)$, obviously, are not affected by $N_{\text{–CH2–}}$. However, the limitation in the number of data available must be considered, such that final conclusions cannot be drawn yet without further data

6 | CONCLUSION

Industrial processing often involves rapid cooling, which results in crystallization of semicrystalline polymers including PA 12 at high supercooling. However, the long methylene unit sequence in the repeat unit and low density of amide groups classify PA 12 as a rather fast crystallizing polymer, and therefore analysis of crystallization at such deep-supercooling is not easily accessible by conventional DSC. By employing FSC, with the capability for fast cooling and heating, PA 12 can be quenched to the glassy state, then crystal nucleation and crystallization at low and high supercooling can be investigated. Due to the limited enthalpy of formation and disappearance of nuclei, Tammann's two-stage crystal nuclei development method is the strategy of choice for investigating homogeneous crystal nucleation.

Two critical cooling rates are determined for PA 12. The first critical cooling rate for suppressing crystallization and the second critical cooling rate for suppressing nucleation are 300 and 10,000 K/s, respectively. In addition, the *CHR* for preventing crystallization of a non-nucleated sample on heating is determined as 10,000 K/s.

A bimodal distribution of the half-time of crystallization as a function of crystallization temperature is observed for PA 12, which shows two minimum values at 333 K, being around 0.05 s, and 383 K, being around 0.8 s. Furthermore, the shortest half-time of nucleation as a function of crystallization temperature is also measured, being around 0.0005 s at 333 K.

By comparing the crystallization kinetics of PA 12 with literature data of other polyamides of higher amide-group density, it appears that the rate of homogeneous crystal nucleation increases with the number of methylene groups between neighbored amide groups in the chain.

ACKNOWLEDGMENTS

Open Access funding enabled and organized by Projekt DEAL. Rui Zhang and Evgeny Zhuravlev thanks for support by Functional Materials Rostock e.V., Germany. Evgeny Zhuravlev acknowledges support by the Deutsche Forschungsgemeinschaft (DFG, SPP2122 program, project ZE 661/3-1). Christoph Schick acknowledges financial support from the Ministry of Education and Science of the Russian Federation, grant 14.Y26.31.0019.

DATA AVAILABILITY STATEMENT

The data that support the findings of this study are available from the corresponding author upon reasonable request.

ORCID

Rui Zhang https://orcid.org/0000-0002-4441-4761
Katalee Jariyavidyanont https://orcid.org/0000-0001-8240-126X
Mengxue Du https://orcid.org/0000-0002-1303-6788
Evgeny Zhuravlev https://orcid.org/0000-0002-4185-8017
Christoph Schick https://orcid.org/0000-0001-6736-5491

REFERENCES

[1] W. Alewelt, *Technische Thermoplaste: Polyamide: mit 251 Tabellen/die Autoren: W. Alewelt*, München, Hanser Verlag, **1998**.
[2] "Nylon 12 (NYLON12) Heat Capacity, Enthalpy, Entropy, Gibbs Energy: Datasheet from "The Advanced THermal Analysis System (ATHAS) Databank – Polymer Thermodynamics" Release 2014 in SpringerMaterials (http://materials.springer.com/polymerthermodynamics/docs/athas_0023)".
[3] T. Fornes, D. Paul, *Macromolecules* **2004**, *37*, 7698.
[4] A. Salazar, A. Rico, J. Rodríguez, J. Segurado Escudero, R. Seltzer, F., *Eur. Polym. J.* **2014**, *59*, 36.
[5] Z. Liu, Y. Wang, B. Wu, C. Cui, Y. Guo, C. Yan, *Int. J. Adv. Manuf. Technol.* **2019**, *102*, 2877.
[6] F. Neugebauer, V. Ploshikhin, J. Ambrosy, G. Witt, *J. Therm. Anal. Calorim.* **2016**, *124*, 925.
[7] C. Plummer, J.-E. Zanetto, P.-E. Bourban, J.-A. Månson, *Colloid Polym. Sci.* **2001**, *279*, 312.
[8] A. A. Minakov, C. Schick, *Rev. Sci. Instrum.* **2007**, *78*, 073902.
[9] A. Wurm, M. Ismail, B. Kretzschmar, D. Pospiech, C. Schick, *Macromolecules* **2010**, *43*, 1480.
[10] D. Mileva, R. Androsch, E. Zhuravlev, C. Schick, *Polymer* **2012**, *53*, 3994.

[11] A. Mollova, R. Androsch, D. Mileva, C. Schick, A. Benhamida, *Macromolecules* **2013**, *46*, 828.
[12] Y. Furushima, M. Nakada, K. Ishikiriyama, A. Toda, R. Androsch, E. Zhuravlev, C. Schick, *J. Polym. Sci., Part B: Polym. Phys.* **2016**, *54*, 2126.
[13] F. Paolucci, D. Baeten, P. Roozemond, B. Goderis, G. Peters, *Polymer* **2018**, *155*, 187.
[14] A. M. Gohn, J. Seo, T. Ferris, P. Venkatraman, E. J. Foster, A. M. Rhoades, *Thermochim. Acta* **2019**, *677*, 99.
[15] T. Wang, X. Li, R. Luo, Y. He, S. Maeda, Q. Shen, W. Hu, *Thermochim. Acta* **2020**, *690*, 178667.
[16] X. Li, Y. He, X. Dong, X. Ren, H. Gao, W. Hu, *Polymer* **2020**, *189*, 122165.
[17] R. Zhang, E. Zhuravlev, J. R. W. P. Schmelzer, R. Androsch, C. Schick, *Macromolecules* **2020**, *53*, 5560.
[18] K. Jariyavidyanont, E. Zhuravlev, C. Schick, R. Androsch, *Polym. Cryst.* **2021**, *4*, e10149(1).
[19] A. M. Gohn, A. M. Rhoades, N. Wonderling, T. Tighe, R. Androsch, *Thermochim. Acta* **2017**, *655*, 313.
[20] C. Fischer, A. Seefried, D. Drummer, *Polym. Eng. Sci.* **2017**, *57*, 450.
[21] A. M. Rhoades, N. Wonderling, C. Schick, R. Androsch, *Polymer* **2016**, *106*, 29.
[22] A. M. Rhoades, J. L. Williams, R. Androsch, *Thermochim. Acta* **2015**, *603*, 103.
[23] R. Androsch, C. Schick, J. W. P. Schmelzer, *Eur. Polym. J.* **2014**, *53*, 100.
[24] I. Kolesov, D. Mileva, R. Androsch, C. Schick, *Polymer* **2011**, *52*, 5156.
[25] D. Cavallo, L. Gardella, G. C. Alfonso, G. Portale, L. Balzano, R. Androsch, *Colloid Polym. Sci.* **2011**, *289*, 1073.
[26] E. Zhuravlev, J. W. P. Schmelzer, B. Wunderlich, C. Schick, *Polymer* **2011**, *52*, 1983.
[27] D. Mileva, A. Monami, D. Cavallo, G. C. Alfonso, G. Portale, R. Androsch, *Macromol. Mater. Eng.* **2013**, *298*, 938.
[28] G. V. Poel, D. Istrate, V. Mathot, *Fast Scanning Calorimetry*, Springer, New York, **2016**, p. 611.
[29] M. van Drongelen, T. Meijer-Vissers, D. Cavallo, G. Portale, G. V. Poel, R. Androsch, *Thermochim. Acta* **2013**, *563*, 33.
[30] L. Li, M. H. Koch, W. H. de Jeu, *Macromolecules* **2003**, *36*, 1626.
[31] C. Schick, R. Androsch, J. W. P. Schmelzer, *J. Phys. Condens. Matter* **2017**, *29*, 453002.
[32] R. Androsch, C. Schick, *Crystal Nucleation of Polymers at High Supercooling of the Melt*. (Eds: F. Auriemma, G. Alfonso, C. de Rosa), Polymer Crystallization I. Advances in Polymer Science, vol. 276, Springer, Cham **2015**. https://doi.org/10.1007/12_2015_325
[33] R. Androsch, M. L. Di Lorenzo, C. Schick, *Macromol. Chem. Phys.* **2017**, *219*, 1700479.
[34] A. Toda, R. Androsch, C. Schick, *Polymer* **2016**, *91*, 239.
[35] C. Schick, R. Androsch, *Polym. Cryst.* **2018**, *1*, e10036.
[36] G. Tammann, *Z Phys. Chem.* **1898**, *25*, 41.
[37] E. Zhuravlev, J. W. P. Schmelzer, A. S. Abyzov, V. M. Fokin, R. Androsch, C. Schick, *Cryst. Growth Des.* **2015**, *15*, 786.
[38] R. Zhang, E. Zhuravlev, R. Androsch, C. Schick, *Polymer* **2019**, *11*, 890.
[39] E. Zhuravlev, C. Schick, *Thermochim. Acta* **2010**, *505*, 1.
[40] A. Minakov, A. Van Herwaarden, W. Wien, A. Wurm, C. Schick, *Thermochim. Acta* **2007**, *461*, 96.
[41] C. Schick, V. Mathot, *Fast scanning calorimetry*, New York, Springer International Publishing **2016**.
[42] A. A. Minakov, C. Schick, *Thermochim. Acta* **2018**, *660*, 82.
[43] A. A. Minakov, C. Schick, *J. Chem. Phys.* **2018**, *149*, 074503.
[44] A. Toda, M. Hikosaka, K. Yamada, *Polymer* **2002**, *43*, 1667.
[45] J. E. K. Schawe, G. Strobl, *Polymer* **1998**, *39*, 3745.
[46] Y. Furushima, S. Kumazawa, H. Umetsu, A. Toda, E. Zhuravlev, C. Schick, *Polymer* **2017**, *109*, 307.
[47] Y. Furushima, C. Schick, A. Toda, *Polym. Cryst.* **2018**, *1*, 1.
[48] B. Sauer, W. Kampert, E. N. Blanchard, S. Threefoot, B. Hsiao, *Polymer* **2000**, *41*, 1099.
[49] R. Androsch, E. Zhuravlev, C. Schick, *Polymer* **2014**, *55*, 4932.
[50] K. Nishida, E. Zhuravlev, B. Yang, C. Schick, Y. Shiraishi, T. Kanaya, *Thermochim. Acta* **2015**, *603*, 110.
[51] T. Mukhametzyanov, J. W. P. Schmelzer, E. Yarko, A. Abdullin, M. Ziganshin, I. Sedov, C. Schick, *Polymer* **2021**, *13*, 13.
[52] D. Mileva, R. Androsch, E. Zhuravlev, C. Schick, B. Wunderlich, *Polymer* **2012**, *53*, 277.
[53] E. Zhuravlev, A. Wurm, P. Pötschke, R. Androsch, J. W. P. Schmelzer, C. Schick, *Eur. Polym. J.* **2014**, *52*, 1.
[54] R. Androsch, C. Schick, A. M. Rhoades, *Macromolecules* **2015**, *48*, 8082.
[55] B. Wunderlich, *Macromolecular Physics*, Elsevier, Amsterdam, **2012**.
[56] A. Wurm, E. Zhuravlev, K. Eckstein, D. Jehnichen, D. Pospiech, R. Androsch, B. Wunderlich, C. Schick, *Macromolecules* **2012**, *45*, 3816.
[57] Y. Furushima, S. Kumazawa, H. Umetsu, A. Toda, E. Zhuravlev, A. Wurm, C. Schick, *J. Appl. Polym. Sci.* **2017**, *134*, 134.
[58] J. Gibbs, *The Collected Papers: Thermodynamics*, Vol. 1, Longmans, Green and Co., New York **1928**.
[59] V. M. Fokin, E. D. Zanotto, N. S. Yuritsyn, J. W. P. Schmelzer, *J. Non-Cryst. Solids* **2006**, *352*, 2681.
[60] J. D. Hoffman, J. I. Lauritzen, *Phys. Chem.* **1961**, *65*, 297.
[61] J. D. Hoffman, G. T. Davis, J. I. Lauritzen, *Treatise on Solid State Chemistry*, Springer, Berlin, **1976**, p. 497.
[62] J. D. Hoffman, *Polym. Eng. Sci.* **1964**, *4*, 315.
[63] R. T. Tol, A. A. Minakov, S. A. Adamovsky, V. B. F. Mathot, C. Schick, *Polymer* **2006**, *47*, 2172.
[64] Q. Zhang, Z. Zhang, H. Zhang, Z. Mo, *J. Polym. Sci., Part B: Polym. Phys.* **2002**, *40*, 1784.
[65] "Nylon 6 (NYLON6) Heat Capacity, Enthalpy, Entropy, Gibbs Energy: Datasheet from "The Advanced THermal Analysis System (ATHAS) Databank – Polymer Thermodynamics" Release 2014 in SpringerMaterials (https://materials.springer.com/polymerthermodynamics/docs/athas_0024)".
[66] "Nylon 6,6 α (NYLON66) Heat Capacity, Enthalpy, Entropy, Gibbs Energy: Datasheet from "The Advanced THermal Analysis System (ATHAS) Databank – Polymer Thermodynamics" Release 2014 in SpringerMaterials (https://materials.springer.com/polymerthermodynamics/docs/athas_0027)".
[67] "Nylon 6,10 (NYLON610) Heat Capacity, Enthalpy, Entropy, Gibbs Energy: Datasheet from "The Advanced THermal Analysis System (ATHAS) Databank – Polymer Thermodynamics" Release 2014 in SpringerMaterials (https://materials.springer.com/polymerthermodynamics/docs/athas_0025)".
[68] "Nylon 6,12 (NYLON612) Heat Capacity, Enthalpy, Entropy, Gibbs Energy: Datasheet from "The Advanced THermal Analysis System (ATHAS) Databank – Polymer Thermodynamics"

Release 2014 in SpringerMaterials (http://materials.springer.com/polymerthermodynamics/docs/athas_0026)".
[69] "Nylon 11 (NYLON11) Heat Capacity, Enthalpy, Entropy, Gibbs Energy: Datasheet from "The Advanced THermal Analysis System (ATHAS) Databank – Polymer Thermodynamics" Release 2014 in SpringerMaterials (http://materials.springer.com/polymerthermodynamics/docs/athas_0022)".
[70] J. E. Mark, *Polymer Data Handbook*, Oxford University Press, New York **1999**.
[71] C. Carfagna, V. Busico, V. Salerno, M. Vacatello, *Thermochim. Acta* **1980**, *37*, 31.
[72] C. Carfagna, M. Vacatello, P. Corradini, *J. Polym. Sci., Polym. Chem. Ed.* **1977**, *15*, 1.
[73] R. Gaymans, S. Harkema, *J. Polym. Sci., Polym. Phys. Ed.* **1977**, *15*, 587.
[74] N. S. Murthy, *J. Polym. Sci., Part B: Polym. Phys.* **2006**, *44*, 1763.

SUPPORTING INFORMATION

Additional supporting information may be found in the online version of the article at the publisher's website.

How to cite this article: R. Zhang, K. Jariyavidyanont, M. Du, E. Zhuravlev, C. Schick, R. Androsch, *J. Polym. Sci.* **2022**, *60*(5), 842. https://doi.org/10.1002/pol.20210813